JCTC Journal of Chemical Theory and Computation

Article

pubs.acs.org/JCTC

Mechanism of Spin−Orbit Effects on the Ligand NMR Chemical Shift in Transition-Metal Complexes: Linking NMR to EPR

Jan Vícha,[†,‡] Michal Straka,[†,§] Markéta L. Munzarová,*[,†,∥] and Radek Marek*[,†,‡,∥]

[†]CEITEC - Central European Institute of Technology, Masaryk University, Kamenice 5/A4, CZ-62500 Brno, Czech Republic

[‡]National Center for Biomolecular Research, Faculty of Science, Masaryk University, Kamenice 5/A4, CZ-62500 Brno, Czech Republic

[§]Institute of Organic Chemistry and Biochemistry of the ASCR, Flemingovo nám. 2, CZ-16610 Praha, Czech Republic

[∥]Department of Chemistry, Faculty of Science, Masaryk University, Kamenice 5, CZ-62500 Brno, Czech Republic

Supporting Information

ABSTRACT: Relativistic effects play an essential role in understanding the nuclear magnetic resonance (NMR) chemical shifts in heavy-atom compounds. Particularly interesting from the chemical point of view are the relativistic effects due to heavy atom (HA) on the NMR chemical shifts of the nearby light atoms (LA), referred to as the HALA effects. The effect of Spin−Orbit (SO) interaction originating from HA on the nuclear magnetic shielding at a neighboring LA, σ^{SO}, is explored here in detail for a series of d^6 complexes of iridium. Unlike the previous findings, the trends in σ^{SO} observed in this study can be fully explained neither in terms of the s-character of the HA-LA bonding nor by trends in the energy differences between occupied and virtual molecular orbitals (MOs). Rather, the σ^{SO} contribution to the total NMR shielding is found to be modulated by the d-orbital participation of the heavy atom (Ir) in the occupied and virtual spin−orbit *active* MOs, i.e., those which contribute significantly to the σ^{SO}. The correlation between the d-character of σ^{SO}-active MOs and the size of the corresponding SO contribution to the nuclear magnetic shielding constant at LA is so tight that the magnitude of σ^{SO} can be predicted in a given class of compounds on the basis of d-orbital character of relevant MO with relative error smaller than 15%. This correspondence is supported by an analogy between the perturbation theory expressions for the spin−orbit induced NMR σ-tensor and those for the EPR g-tensor as well as the A-tensor of the ligand. This correlation is demonstrated on a series of d^5 complexes of iridium. Thus, known qualitative relationships between electronic structure and EPR parameters can be newly applied to reproduce, predict, and understand the SO-induced contributions to NMR shielding constants of light atoms in heavy-atom compounds.

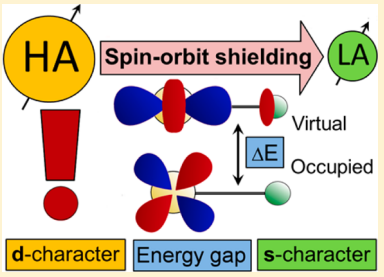

1. INTRODUCTION

Relativistic effects play an important role in various spectroscopic techniques including nuclear magnetic resonance (NMR), especially for systems with heavy atoms (HA). The importance of relativistic effects increases with the increasing atomic number Z of a HA, and besides influencing the NMR signal of the HA itself (HAHA effect), the NMR chemical shifts of the light atoms (LA) neighboring the HA center are affected as well (HALA effect). Whereas the HAHA effect is strongly influenced by both scalar-relativistic effects and spin−orbit (SO) coupling, the HALA effect tends to be dominated by SO coupling.[1] In the present work we extend the previous knowledge of the mechanism of the SO-HALA effect on the spin−orbit nuclear shielding tensor (σ^{SO}-tensor) in a way illuminating a so-far overlooked relationship to the electronic g-tensor (g-tensor) and ligand hyperfine coupling tensor (A-tensor) of the electron paramagnetic resonance (EPR).

To the best of our knowledge, the first reports of the SO-HALA effect are those by Nakagawa, Sinada, and Obinata, 1967,[2] by Nomura, Takeuschi, and Nakagawa, 1969,[3] and by Cheremisin and Schastnev, 1969.[4] In the contributions by Nakagawa et al., a sizable contribution of a third-order perturbation term, referred to as 'spin-polarization' shift (*LS* shift) has been postulated to explain anomalous chemical shifts of halobenzenes. The mechanism of this effect was suggested to be analogous to that of the indirect spin−spin coupling between nuclei.[3] Cheremisin and Schastnev developed a method for calculating the SO-induced contributions to the NMR chemical shift and predicted small contributions for chlorine-substituted, essential contributions for bromine-substituted, and predominant contributions for iodine-substituted methane. In 1987, Pyykkö, Görling, and Rösch identified relativistic contributions using relativistically parametrized Extended Hückel Theory within the second-order perturbation theory and coined the effect as a 'heavy-atom chemical shift'.[5]

In 1997, Kaupp et al. reported the first study of both SO-coupling and electron-correlation effects on the ^{13}C NMR chemical shifts in halomethyl cations. It was shown that the

Received: August 14, 2013
Published: February 11, 2014

   dx.doi.org/10.1021/ct400726y | *J. Chem. Theory Comput.* 2014, 10, 1489−1499

trend of the decreasing ^{13}C NMR chemical shifts with increasing atomic number of the halogen is due to the shielding contribution induced by the SO coupling at HA.[6] In a subsequent work in 1998, Kaupp et al. found that the magnitude of the SO-induced contribution to the NMR chemical shift of LA in neighborhood of HA, σ^{SO}, increases with the growing s-character of LA in the molecular orbital (MO) representing the HA-LA bond.[7] The interpretation of the latter finding as well as of a notable observation of Karplus-like dependence of the SO-HALA effects on β-protons in iodoethane was done by demonstrating the analogy between the mechanism of the SO-HALA effect and the mechanism of indirect nuclear spin−spin coupling suggested already by Nomura et al. in 1969.[3] The following physical picture has been drawn, cf. Figure 1: In the presence of an external

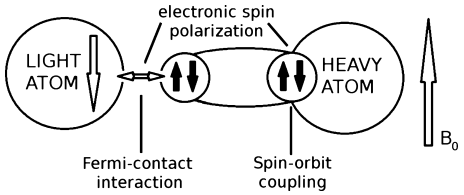

Figure 1. A simplified scheme of the Fermi-contact mechanism of HALA effect - along the lines of ref 7.

magnetic field, the SO operator on HA mixes the singlet and the triplet states and hence induces spin polarization in the molecule. The polarized spin density in turn interacts with the nuclear spin of the LA via the Fermi-contact (FC) mechanism and induces an additional nuclear shielding or deshielding at the LA. The FC mechanism becomes more effective with increasing s-character of the HA-LA bonding, since the FC matrix element is proportional to the spin density at the LA nucleus. The reason is that only s-type orbitals of a particular atom have a nonzero density at its nucleus.[7,8] In 1998, Wolff and Ziegler[9] and Minaev et al.[10] pinpointed that the efficiency of the Fermi-contact mechanism is codetermined by the internuclear separation between HA and LA.

As a second factor influencing the size of σ^{SO}, energy gap between the highest occupied molecular orbital (HOMO) and lowest unoccupied molecular orbital (LUMO) energies has been considered. Wolf and Ziegler, 1998, in their study of 5d transition-metal carbonyls noted that σ^{SO} should decrease with increasing HOMO−LUMO energy gap, but the actual trend found was a reverse one.[9] Motivated by the observation of remarkably large spin−orbit effects on ^{1}H NMR shielding constants in d^6 Co complexes by Hegetschweiler et al. in 2004,[11] in 2009 Hyvärinen et al. published a comparative study of Co, Rh, and Ir d^6 complexes, in which σ^{SO} was indeed found inversely proportional to the energy gaps.[12] Energy-gap arguments were also used to interpret the dependence of the SO-HALA effects on the bond length in actinide fluoro-chloride complexes studied by Straka et al.[13] as well as the trends in halide nuclear magnetic shielding constants of CuX, AgX, and AuX in a recent work by Yoshizawa and Sakaki.[14]

The third factor to be considered for interpreting σ^{SO} is the role played by the SO operator itself, which has been previously somewhat overlooked.[15] We are aware of only a few studies considering explicitly the latter, especially those by Wolf and Ziegler, 1998,[9] and by Neto et al., 2009.[15] Neto et al. considered the effect of hyperconjugative interactions in halogen substituted cyclohexane and pyrane derivatives on the SO matrix element. Wolf and Ziegler concluded that in a series of 5d transition-metal carbonyl compounds, the decisive factor for the size of the σ^{SO}-tensor is the balance between the $\sigma-\sigma$ and $\pi-\pi$ interactions between the metal and the ligand, of which only the former ($\sigma-\sigma$) is reflected in the Fermi-contact contribution to the NMR chemical shift.[9] Two additional studies parallelizing the size of σ^{SO} and the covalence of the metal−ligand bond[16,17] are closely related to the work by Wolf and Ziegler. The influence of the covalent character of bonding may seem clear; however, a more covalent bonding infers intuitively also a larger separation of occupied and virtual MOs, hence a lower σ^{SO} due to larger energy denominators,[12] while opposite was found.

The present work was motivated by our desire to acquire a complex understanding of the trends in σ^{SO} of the light ligand atoms in transition-metal complexes with respect to the character of the metal−ligand bond,[1,16,17] while persisting the compatibility with the previously explored factors influencing the σ^{SO}, i.e., the energy gap, the Z^2-dependence, and the light-atom hybridization factors. We have done so while analyzing the influence of the effect of ligand *trans* to the light NMR nucleus in question, i.e., the *trans* effect,[18] on the size of σ^{SO}, observed in our previous study.[19] It is known that a modification of a ligand in a transition-metal complex influences mainly the bonding of the ligand occupying the position *trans* to the modifying ligand, without changing the hybridization of the *trans* ligand itself.[18] This phenomenon has wide applications in the chemical synthesis.[20] We tune the electronic structure at HA, which was previously shown to influence the magnitude of σ^{SO},[21] via modification of the bonding in the *trans* position to the light NMR spectator atom. We demonstrate that, due to the *trans* effect, the different ligands *trans* to the light NMR spectator atom influence the participation of the metal *d*-orbitals in the MOs which − via the Spin−Orbit Fermi-Contact (SO/FC) mechanism (Figure 1) − modulate σ^{SO} at the nucleus of the light atom.

We further rationalize the role of the metal d-character in the SO-induced nuclear magnetic shielding in combination with the other factors: the Z^2-dependence, the energy-denominators, and the LA hybridization. This is done on the basis of an analogy between the perturbation theory expressions for the σ^{SO}-tensor and for the EPR g- and A-tensor. By this we complement earlier observations of common structural and electronic factors influencing (i) σ^{SO} and spin−spin coupling[3,7] and (ii) EPR g- and A-tensor.[22]

2. COMPUTATIONAL DETAILS

Structure and Bonding. The main part of this study was performed on the model complex [$Ir^{III}Cl_4$(BAPH)(DMSO)], abbreviated as IrBAP (**1**), with dimethyl sulfoxide (DMSO) and 6-benzylaminopurine (BAP)[23,24] as axial ligands. As in our previous study,[19] the Ir−S bond length in IrBAP was altered over the interval of 25 pm in a 5 pm step [from 2.13 Å (short, **1S**) to 2.38 Å (long, **1L**)] around the equilibrium value (2.23 Å). While the Ir−S bond was constrained to the desired length, the rest of the molecular geometry was optimized at the PBE0[25,26]/def2-TZVPP[27]/def2-ECP[28] level of theory employing Turbomole 6.3.1.[29] COSMO description (COnductor-like Screening MOdel)[30] of solvent effects, with dimethylformamide (DMF) used as solvent (ε = 37, r_{solv} = 3.13 Å), was adopted throughout geometry optimizations. This level of theory (PBE0/def2-TZVPP/COSMO) was justified in our previous

dx.doi.org/10.1021/ct400726y | J. Chem. Theory Comput. 2014, 10, 1489−1499

work, where it correctly reproduced the obtained experimental values.[19] Therefore it was maintained here as well.

To analyze the changes in the d-character of MOs along with the *trans* effect in a broader range of iridium compounds, Ir complexes with various sulfur or oxygen based ligands were constructed *in silico*, and their geometries were optimized at the PBE0/def2-TZVPP/def2-ECP level of theory *in vacuo* to avoid the influence of different solvent effects in analysis. For this purpose, also the IrBAP molecule (**1**) was reoptimized *in vacuo*.

Calculation and Analysis of NMR Shielding Constants. For the experimental ^{1}H, ^{13}C, and ^{15}N NMR chemical shifts of **1** and for the preliminary analysis of the changes in nuclear magnetic shielding on N9 during the stretching of the bond to *trans* substituent, see ref 19. In the current work we focused on σ^{SO} of N9 that was shown to be the most influenced by the changes in *trans* substituent bonding (~5 times more as compared to the changes in the nonrelativistic or scalar-relativistic contribution to the shielding constant of this atom).[19]

Nuclear magnetic shielding constants for the IrBAP molecule were calculated at the SO-ZORA (Zeroth-Order Regular Approximation)[31,32] level of theory using the ADF2012 code.[33] The exchange-correlation functional based on the PBE0 with a user-defined amount of the exact-exchange admixture of 40% (denoted as the PBE40) was employed.[19] We used the TZP basis sets from the ADF library and the COSMO solvent model (DMF solvent, ε = 37, r_{solv} = 3.13 Å) as implemented in ADF2012.[34] The NMR shielding constants for the iridium(III) complexes were calculated in vacuo at the SO-ZORA/PBE40/TZP level of theory.

The analysis of MO contributions to σ^{SO} was performed in MAG 2.1[35,36] code interfaced with Gaussian 09,[37] further referred to as G09. The PBE functional, the def2-SVP basis set for light atoms, and the all-electron Faegri basis set for iridium[38] (Faegri-III, FIII) were used. A perturbation of 0.005 au was set at nitrogen N9 of the purine ligand. The difference between σ^{SO} for ^{15}N in **1S** and **1L**, denoted as $\Delta\sigma^{SO}$, calculated at the PBE/def2-SVP/FIII level of theory using the G09/MAG routines, amounts to 28 ppm. A comparative calculation at the SO-ZORA/PBE40/TZP level of theory resulted in $\Delta\sigma^{SO}$ of 25 ppm. This agreement allowed for MO analyses performed using the G09/MAG at the PBE/def2-SVP/FIII level of theory, cf. below.

Calculation and Analysis of EPR g-Tensor and Ligand Isotropic Hyperfine Coupling (A_{iso}). Calculation of EPR parameters was performed for the hypothetical ionized structures of complexes **1**–**8**, which were obtained from the structures of neutral molecules by removing one electron prior to the geometry optimization. The structures with a positive charge of +1 were optimized at the same level of theory as neutral molecules **1**–**8** employing the unrestricted Kohn–Sham formalism. The optimization of structures of **7** and **8** failed to converge, probably due to a large delocalization of unpaired electron stabilized by the nearby heterocyclic ligand. Therefore, only results for **1**–**6** are presented. The calculation of the EPR parameters (g-tensor, ligand isotropic hyperfine coupling constant) was performed in ADF2013 at the unrestricted SO-ZORA/PBE40/TZP level, invoked by keyword ESR during unrestricted calculation with collinear approximation.[34]

Molecular Orbital and Bonding Analysis. The character and composition of MOs was determined as the net Mulliken population summed over all Gaussian basis functions of a given type, including their mutual overlap populations, employing the pop=allorbitals keyword of G09. The character of particular chemical bonds was quantified using the Natural Bond Orbital (NBO) analysis[39] following the contribution of Natural Atomic Orbitals (NAO) in the corresponding NBO. For the two limiting structures of IrBAP, natural bond orbital analysis was performed by using the NBO code in Version 3.1, as implemented in G09,[37] using the def2-SVP/FIII basis and the implicit DMSO solvent description. In the case of the full set of complexes, we employed the NBO code in Version 5.9 (Gennbo)[40] interfaced with the ADF program[33] along with the PBE40 exchange-correlation functional, the TZP basis, and the ZORA level of calculation in vacuo.

3. RESULTS AND DISCUSSION

3.1. The Specification of Systems and the Character of Bonding. Our systems of interest are eight d^6 complexes of iridium **1**–**8** shown in Figure 2. This selection was motivated

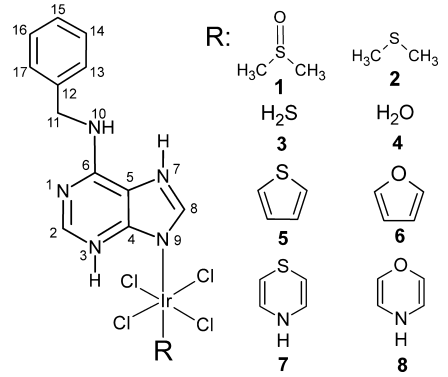

Figure 2. Schematic representation of studied complexes **1**–**8**.

by results of our previous study.[19] The configuration of ligands around the central Ir atom is close to the C_{4v} symmetry. The ligand-field splitting scheme for d orbitals of the central atom in the C_{4v} symmetry is shown in Figure 3. A detailed metal–ligand MO interaction diagram for the O_h symmetry, of which the approximate C_{4v} symmetry of our complexes can be considered

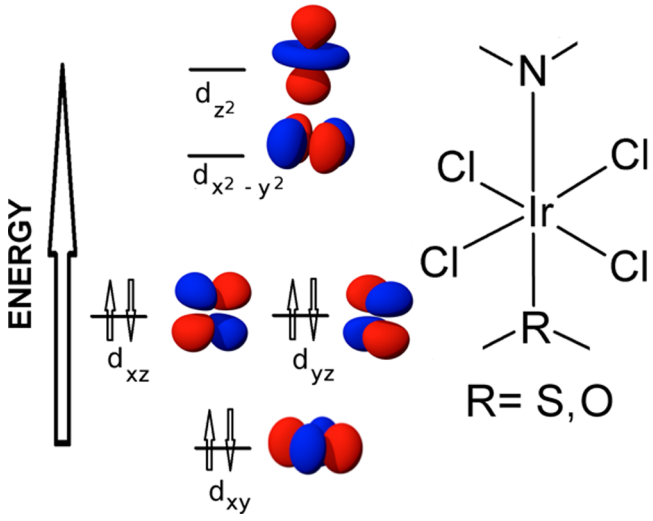

Figure 3. Schematic representation of iridium atomic d orbitals in C_{4v} ligand arrangement as in complexes **1**–**8**.

dx.doi.org/10.1021/ct400726y | J. Chem. Theory Comput. 2014, 10, 1489–1499

as an electronegativity perturbation, is given in Figure S1 of the Supporting Information.

In this study, we concentrate on σ^{SO} of the axially coordinated nitrogen atom of purine, N9, as the light atom, LA, that is together with the S atom bonded to the central atom mainly via the Ir $5d_z^2$ orbital. To study the influence of electronic and structural effects on σ^{SO} (trace) and the σ^{SO}-tensor, we employed two ways of modulating the electronic structure at N9 via ligand in the *trans* position to N9. First, an artificial stretching of the *trans* Ir−S bond in the IrBAP complex (structure **1** in Figure 2) was done to simulate different electronic and bonding situations and to provide a model for different sulfur-based ligands bonded to Ir with different Ir−S bond lengths.[41,42] Second modification presents the direct substitution of the axial DMSO ligand by a series of "soft" (sulfur based) and "hard" (oxygen based) ligands, see complexes **2**−**8** in Figure 2. We start the analysis with the simpler IrBAP model using the two limiting geometries of IrBAP (**1**, cf. Figure 2) corresponding to the Ir−S interatomic distance fixed at 2.13 Å (short - **1S**) and 2.38 Å (long - **1L**) with the rest of the geometry parameters optimized. For details, see the Method section.

3.2. An Analogy between the NMR SO-Shielding Tensor, the EPR g-Tensor, and the EPR Hyperfine Coupling Tensor. *NMR SO-Shielding Tensor (σ^{SO}-Tensor).* The spin−orbit correction to the NMR shielding tensor (σ^{SO}) is a third-order property which arises from the interplay of the spin−orbit operator $\hat{\mathbf{H}}^{SO}$ with the orbital angular momentum operator $\hat{\mathbf{L}}_v$ and the Fermi-contact as well as spin-dipolar operators ($\hat{\mathbf{H}}^{FC}$ and $\hat{\mathbf{H}}^{SD}$). As the SD contribution is usually rather small for the light atoms,[43,44] the FC term dominates the σ^{SO}. One of the $\boldsymbol{\sigma}^{SO/FC}$ implementations is based on a combination of finite-field perturbation theory (FFPT) and the SOS-DFPT approach for nonrelativistic chemical shift calculations. There the Fermi-contact operator is included in the 'ground state' Hamiltonian by means of a finite perturbation parameter λ. The leading contribution to the σ^{SO}-tensor is then given by[45]

$$\sigma_{vu}^{p} = \frac{i}{\lambda_N}\left[\frac{e\hbar}{2mc}B_v \sum_{k}^{occ(\alpha)}\sum_{a}^{virt(\alpha)} \frac{\langle\varphi_k^{\alpha}(\lambda_N)|\hat{\mathbf{L}}_v|\varphi_a^{\alpha}(\lambda_N)\rangle\langle\varphi_a^{\alpha}(\lambda_N)|\hat{\mathbf{H}}_u^{SO}|\varphi_k^{\alpha}(\lambda_N)\rangle}{\varepsilon_k - \varepsilon_a}\right] - \frac{i}{\lambda_N}\left[\frac{e\hbar}{2mc}B_v \sum_{k}^{occ(\beta)}\sum_{a}^{virt(\beta)} \frac{\langle\varphi_k^{\beta}(\lambda_N)|\hat{\mathbf{L}}_v|\varphi_a^{\beta}(\lambda_N)\rangle\langle\varphi_a^{\beta}(\lambda_N)|\hat{\mathbf{H}}_u^{SO}|\varphi_k^{\beta}(\lambda_N)\rangle}{\varepsilon_k - \varepsilon_a}\right] \quad (1)$$

The parts of eq 1 for α spin and for β spin have different signs. This leads to the difference between α and β contributions to the spin−orbit correction to the magnetic shielding depending on the spin-polarization in the system.[45]

EPR g-Tensor. The leading SO contribution to the g-tensor arises due to the interplay of the spin−orbit operator $\hat{\mathbf{H}}^{SO}$ at the heavy atom and the orbital angular momentum operator $\hat{\mathbf{l}}_{iO}$ of electron i with respect to the gauge origin O:[46]

$$\Delta g_{SO/OZ,uv} = \frac{\alpha^2}{2} g_e \left[\sum_{k}^{occ(\alpha)}\sum_{a}^{virt(\alpha)} \frac{\langle\psi_k^{\alpha}|\hat{\mathbf{H}}_v^{SO}|\psi_a^{\alpha}\rangle\langle\psi_a^{\alpha}|\hat{\mathbf{l}}_{O,u}|\psi_k^{\alpha}\rangle}{\epsilon_k^{\alpha} - \epsilon_a^{\alpha}} - \sum_{k}^{occ(\beta)}\sum_{a}^{virt(\beta)} \frac{\langle\psi_k^{\beta}|\hat{\mathbf{H}}_v^{SO}|\psi_a^{\beta}\rangle\langle\psi_a^{\beta}|\hat{\mathbf{l}}_{O,u}|\psi_k^{\beta}\rangle}{\epsilon_k^{\beta} - \epsilon_a^{\beta}}\right] \quad (2)$$

Common factors of eqs 1 and 2 are the matrix elements over the spin−orbit operator $\hat{\mathbf{H}}^{SO}$ as well as the angular momentum operators $\hat{\mathbf{L}}_v$ or $\hat{\mathbf{l}}_{O,u}$ in the nominators and the energy differences $\epsilon_k^{\alpha} - \epsilon_a^{\alpha}$ and $\epsilon_k^{\beta} - \epsilon_a^{\beta}$ in the denominators. Formulas 1 and 2 differ in the additional operation of the Fermi-contact perturbation in (1). This suggests that electronic and structural factors influencing the g-tensor could be similar to those modulating the σ^{SO}-tensor if the Fermi-contact part of the mechanism is considered constant.

EPR Hyperfine Coupling Tensor (A-Tensor). The isotropic hyperfine coupling constant (HFCC) for the ligand nucleus N can be written as[47,48]

$$A_{iso}(N) = A_{FC}(N) + A_{PC}(N) \quad (3)$$

where the $A_{FC}(N)$ represents the nonrelativistic contribution to the isotropic HFCC due to the Fermi-contact mechanism, and the $A_{PC}(N)$ stands for the relativistic pseudocontact correction arising from the SO coupling. The explicit formulation for $A(N)$ can be found in ref 47. The contribution $A_{FC}(N)$ is determined by the expectation value of the FC operator at the ligand nucleus N, which is directly proportional to the spin density at this nucleus. The latter is determined by (i) the amount of unpaired spin at the transition metal and (ii) the efficiency of spin-delocalization and spin-polarization mechanisms.[49] The extent of the spin delocalization can be expected to parallel the efficiency of the SO-HALA transfer (σ^{SO}). Trends in pseudocontact contribution, $A_{PC}(N)$, should parallel those for the σ^{SO} of the ligand atom (N) even more, since both the $A_{PC}(N)$ and the σ^{SO} are determined by the interplay of the SO coupling at the metal ($\hat{\mathbf{H}}^{SO}$) and the Fermi-contact term at the ligand ($\hat{\mathbf{H}}^{FC}$).

Common Factors Influencing Considered Magnetic Resonance Parameters. In the field of EPR, the understanding of electronic and structural effects on the g-tensor has a long history, since this observable is directly measurable. The g-tensor deviates from the free electron g-value predominantly due to the spin−orbit coupling that mixes the pure spin ground state with certain excited states.[50] The latter interaction can be split into the magnetic couplings between individual occupied and virtual molecular orbitals.[51]

In a simplified way, the components of the g-tensor can be written as[52]

$$g_{ij} = 2.0023\delta_{ij} - 2\xi_{n,l}\Lambda_{ij} \quad (4)$$

where

$$\Lambda_{ij} = \sum_{m} \frac{\langle\phi_0|\hat{l}_i|\phi_m\rangle\langle\phi_m|\hat{l}_j|\phi_0\rangle}{E_m - E_0} \quad (5)$$

Here δ_{ij} is equal to 1 for $i = j$ and is zero otherwise, while $\xi_{n,l}$ is the single-electron SO-coupling constant which can be extrapolated from the experiment. The $E_m - E_0$ values correspond to the energy differences between the orbital ϕ_0 of the unpaired electron (SOMO) and other valence (doubly

Table 1. Calculated σ^{SO} for N9 and the Composition of the Ir−S and Ir−N9 Natural Bonding Orbitals (NBO)

		Ir−S NBO					Ir−N9 NBO				
		iridium (%)		sulfur (%)			iridium (%)		nitrogen (%)		
r(Ir−S)/Å	σ^{SO}(N9)/ppm	sum[a]	d[b]	sum[a]	s[b]	p[b]	sum[a]	d[b]	total[a]	s[b]	p[b]
2.13 (**1S**)	29.5	36	64	64	27	73	11	51	89	30	70
2.18	34.1	34	64	66	26	74	12	51	88	30	70
2.23	38.1	32	64	67	26	74	12	51	88	30	70
2.28	44.0	31	64	69	25	75	13	51	87	30	70
2.33	49.1	30	64	70	24	76	13	52	87	30	70
2.38 (**1L**)	54.2	28	64	72	24	76	14	52	86	30	70

[a]Sum of all NAO contributions for the corresponding atom (Ir, S, or N) to the NBO. [b]Individual atomic shell (s, p, or d) contribution to the particular NBO for the corresponding atom (Ir, S, or N).

Table 2. MO Contributions to σ^{SO} and to the Principal Components of σ^{SO} at N9 (in ppm)[a,b]

	1S (Ir−S 2.13 Å)				**1L** (Ir−S 2.38 Å)				$\Delta\sigma^{SO}$
MO	σ^{SO}	σ^{SO}_{11}	σ^{SO}_{22}	σ^{SO}_{33}	σ^{SO}	σ^{SO}_{11}	σ^{SO}_{22}	σ^{SO}_{33}	σ^{SO}(**1L**) − σ^{SO}(**1S**)
138	−6.2	0.0	−4.7	−14.0	0.0	0.0	0.0	0.0	+6.2
139	+11.4	+0.2	−1.4	+35.3	−4.9	−0.2	−12.3	−2.4	−16.3
140	+1.1	0.0	+2.4	+0.9	+19.1	+0.3	+8.9	+48.1	+18.0
141	+12.6	0.0	+37.8	−0.1	+15.7	−1.0	+44.6	+3.5	+3.1
151	−2.4	−0.6	−3.0	−3.4	+6.0	+0.1	+0.8	+17.2	+8.4
152	−5.3	−0.5	−11.9	−3.5	+4.0	−0.3	+1.5	+10.7	+9.3
Σ_{MO}	+11.2	−0.9	+19.2	+15.2	+39.9	−1.1	+43.4	+77.1	+28.7
sum/MAG	+19.1	−3.5	+20.2	+40.5	+47.5	−8.4	+57.1	+94.9	+28.4
sum/ADF	+29.5	−7.0	+43.3	+52.2	+54.2	−13.4	+82.7	+93.4	+24.7

[a]$\Delta\sigma^{SO} = \sigma^{SO}$(**1L**) − σ^{SO}(**1S**). Only contributions of MOs with $\Delta\sigma^{SO} \geq 3$ ppm are shown (The threshold of 3 ppm corresponds approximately to 10% of total $\Delta\sigma^{SO}$). [b]Values obtained at the PBE/def2-SVP/FIII level of theory using G09/MAG, except for the last line that refers to the PBE40/TZP/SO-ZORA level using ADF2012.

occupied or virtual) orbitals ϕ_m. The elements $\langle\phi_0|\hat{l}_i|\phi_m\rangle$ and $\langle\phi_m|\hat{l}_j|\phi_0\rangle$ couple ϕ_0 and other doubly occupied or virtual orbitals through the angular momentum operator components. Neglecting ligand contributions, each component of the g-tensor can thus be expressed as a sum of contributions corresponding to the magnetic couplings of the SOMO with virtual and doubly occupied MOs of proper symmetry. Each of these magnetic-coupling contributions is proportional to (i) the square of metal d-orbital contribution in the SOMO, (ii) the square of metal atomic d-orbital contribution in the magnetically coupled MO (virtual or doubly occupied), and (iii) the inverse of the energy difference between the two MOs.[53−58]

Since the d-character of the g-tensor-active MOs codetermines the size of the principal components of the g-tensor, and since eqs 1 and 2 contain common matrix elements over $\hat{\mathbf{L}}_v/\hat{l}_{O,u}$ components, then the d-character of σ^{SO}-active MOs should codetermine the size of σ^{SO}. This has two consequences. First, an additional factor to be considered for the size of σ^{SO} is the metal d-character of frontier molecular orbitals involved in the mechanism of the SO-HALA effect. Second, trends in the σ^{SO}-tensor and the d-character may turn to be paralleled by trends in principal components of the g-tensor of related open-shell species, provided that MOs contributing to the g-tensor have a significant resemblance to MOs involved in the SO-shielding mechanism in NMR. Depending on the particular electron configuration and the symmetry of the complex, this may be (but does not have to be) fulfilled for the individual components of the g-tensor.

Composition of frontier molecular orbitals is known to influence also the EPR hyperfine coupling constant for both the metal and the ligand.[59,60] In analogy to the σ^{SO}-tensor and the g-tensor, the HFCC to ligand atom depends on the coefficients of metal d orbitals in the SOMO and magnetically coupled virtual and/or doubly occupied MOs (see Section 3.5).

3.3. Modulation of σ^{SO} and the Propagation of SO Effects (SO/FC Mechanism) to the Light Nucleus in Molecule 1. *The Role of s-Character of LA in the Bonding.* We first explore the modulation of σ^{SO} of N9 in **1** as a function of nitrogen s-character in the Ir−N bonding. The NBO analysis (Table 1) demonstrates that nitrogen s-contribution in the Ir−N bond remains constant upon elongation of the Ir−S bond, while the σ^{SO} varies to a great extent. This is in contrast with previous theoretical observations for main group elements, where changes in σ^{SO} were found to be related mostly to the ligand s-character in bonding.[7] The possible variation of the $\hat{\mathbf{H}}^{FC}$ matrix element can be also explored by visualizing the propagation of spin density induced by imposing a Fermi-contact perturbation at the nitrogen atom.[11] The negligible difference between the spin densities obtained in this way for **1S** and **1L** (Figure S2 in the Supporting Information) suggests that the $\hat{\mathbf{H}}^{FC}$ matrix elements are, within this system, not responsible for the modulation of σ^{SO} upon changing the Ir−S bond length.

MO Analysis of σ^{SO} and the Role of Energy Gap between Occupied and Virtual MOs. In the MO framework, σ^{SO} can be regarded as a sum of magnetic couplings between occupied and virtual MOs, modulated by the energy denominators. The value of σ^{SO} can be broken down to the contributions from individual occupied MOs, and each of such contributions can be further split into individual contributions from magnetic couplings between the given occupied MO and individual virtual MOs*.[61−63]

The results of our MO analysis reveal that in both **1S** and **1L**, the contributions to σ^{SO} from low-lying MOs 1−137 (not

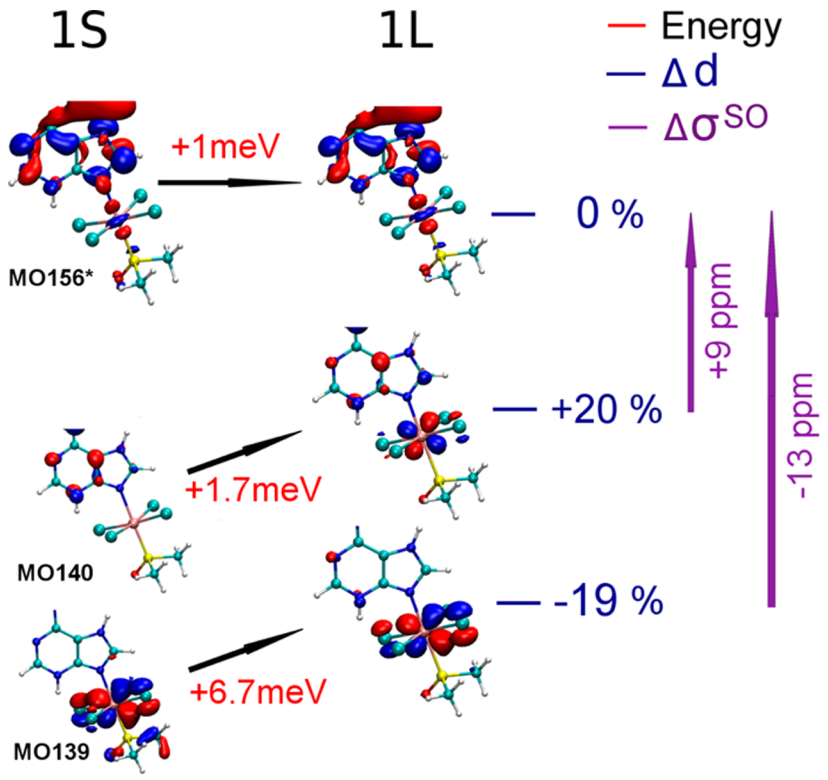

Figure 4. Visualization of MOs 139, 140, and 156*, along with corresponding modulations of the orbital d-character (Δ d-character in %), changes in orbital energies (meV), and modulations of the individual MO-MO* magnetic-coupling contributions to σ_{SO} at N9 ($\Delta\sigma^{SO}$ in ppm), when comparing structures **1S** and **1L**.

shown here) compensate mutually almost perfectly leaving the total σ^{SO} for MOs 1−137 of only 0.6 ppm. This range of MOs includes also some MOs with the σ-bonding character of Ir−N and Ir−S bonds (MOs 120−133, see Figure S3 of the Supporting Information). Although these bonding orbitals are significantly altered by stretching the Ir−S bond and, therefore, might significantly influence σ^{SO}, the sum of their contributions to the modulation of σ^{SO} is vanishingly small. Apparently, these MOs lie too low in energy to allow for their efficient magnetic couplings with suitable virtual MOs.

The major change in σ^{SO} ($\Delta\sigma^{SO}$) upon structural modulation from **1S** to **1L**, (σ^{SO}(**1L**) − σ^{SO}(**1S**)) is mediated by the group of the highest occupied MOs 138−153. We identified six MO contributions to σ^{SO} that vary most between **1S** and **1L**, ($\Delta\sigma^{SO}$ ≥ 3 ppm), see Table 2. These can be divided into two groups: MO 138 and 141 with $\Delta\sigma^{SO}$ between 3 and 6 ppm and MOs 139, 140, 151, and 152 (HOMO-1) with $\Delta\sigma^{SO}$ between 8 and 18 ppm. The latter four MOs are denoted below as the "σ^{SO}-active" MOs since they most efficiently "translate" the changes in the electronic structure into the σ^{SO} at N9. The energy of all four σ^{SO}-active MOs rises upon bond stretching as a result of bond weakening (see Figure S4 of the Supporting Information). This increase in energy is partially responsible for the reduced energy gap between occupied and virtual orbital space and, in turn, affects σ^{SO}. In contrast, energies of the quantitatively most important virtual σ^{SO}-active MOs 158* and 161* decrease upon bond stretching, which results in a further reduction of the energy gap. In the language of the ligand field theory, upon stretching the Ir−S bond, the Ir−S interaction is weakened, and the stabilizing effect of the ligand decreases. This is responsible for weaker ligand field and, in parallel, for the reduced splitting of the d-orbital energy levels (Figure 3) and the reduced energy denominators.

The smaller energy gap for the stretched bond should intuitively lead to a larger σ^{SO} contribution for the particular pair of MOs. However, the physical picture for σ^{SO} is a more complicated one. While some MO → MO* magnetic couplings are indeed connected with an *increase* in $\Delta\sigma^{SO}$ (e.g., MO 140 → MO 156* and MO 151 → MO 158*) upon the structural alteration, others are connected with a *decrease* in $\Delta\sigma^{SO}$ (e.g., MO 139 → MO 156* and MO 151 → MO 161*). All corresponding denominators are actually smaller in **1L** as compared to **1S**. Hence, unlike in refs 12 and 14, for the present case the energy gap arguments themselves are not sufficient for understanding the $\Delta\sigma^{SO}$ modulation.

The Role of the d-Character of HA in the σ^{SO}-Active MOs. We note that all four σ^{SO}-active MOs (MOs 139, 140, 151, and 152) have important contributions from Ir d_{xz} and d_{yz} AOs. Spin−orbit operator mixes the latter predominantly with virtual MOs (156* to 161*) which possess metal d_{z2} and d_{x2-y2} character. Thus, the $\hat{\mathbf{H}}^{SO}$ matrix elements appear to codetermine the size of the σ^{SO}-tensor and its trace σ^{SO} just as the magnetic couplings determine the EPR g- and A-tensors (see Sections 3.2 and 3.5). The pictorial explanation of the σ^{SO} modulation due to the Ir−S bond stretching in complex **1**, $\Delta\sigma^{SO}$, is shown for MOs 139 and 140 in Figure 4 and for MOs 151 and 152 in Figure 5. A more detailed analysis of MO → MO* magnetic couplings, including ligand and metal characters of given MOs and differences for all components of the σ^{SO}-tensor for N9, is given in the Supporting Information (Table S1 for MOs 139 and 140 and Table S2 for MOs 151 and 152).

Let us start our discussion of Figures 4 and 5 by noting that none of the occupied σ^{SO}-active MOs contains appreciable s-

dx.doi.org/10.1021/ct400726y | J. Chem. Theory Comput. 2014, 10, 1489−1499

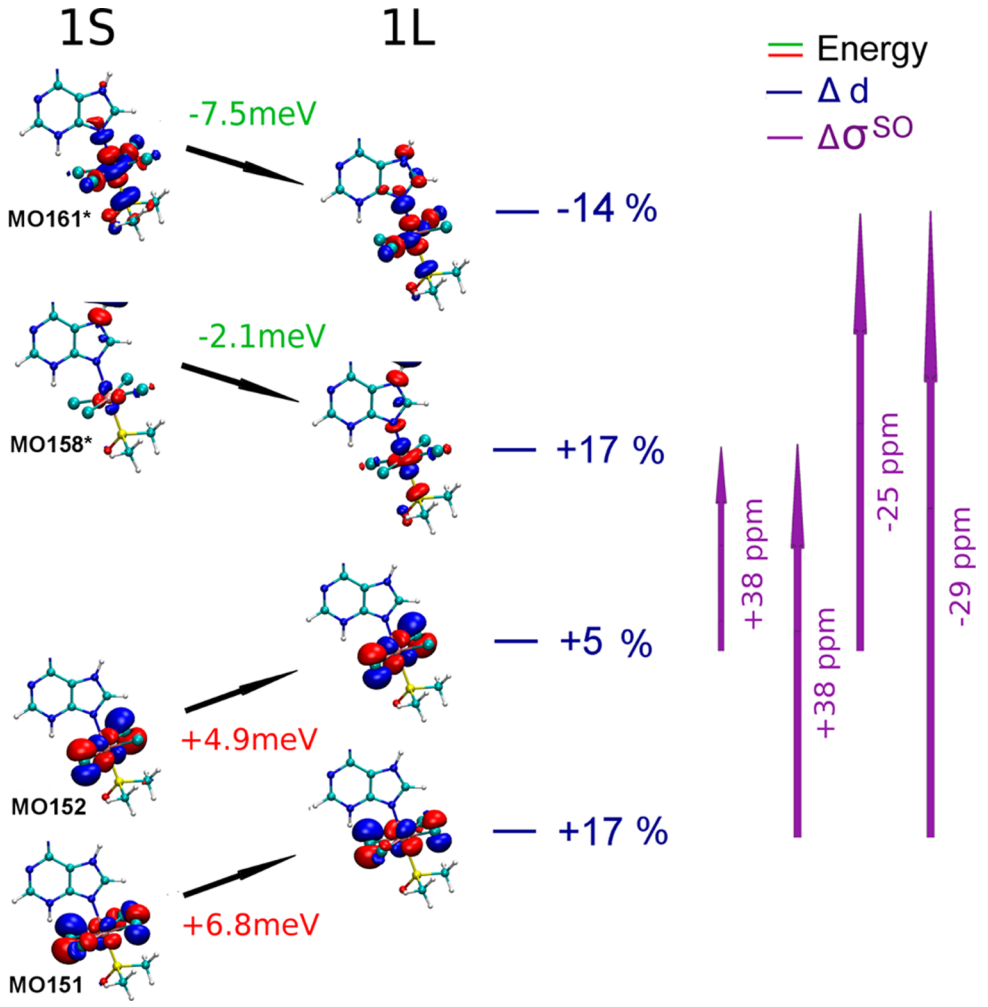

Figure 5. Visualization of MOs 151, 152, 158*, and 161*, along with corresponding modulations of orbital the d-character (Δ d-character in %), changes in orbital energies (meV), and modulations of individual MO-MO* magnetic-coupling contributions to σ_{SO} at N9 ($\Delta\sigma^{SO}$ in ppm), when comparing structures **1S** and **1L**.

character of the nitrogen atom (less than 1%). Only the magnetic couplings of occupied σ^{SO}-active MOs with virtual MOs generate the spin density at the light atom, N9, because virtual σ^{SO}-active MOs contain contributions from hybrid sp atomic orbitals of nitrogen (allowed by symmetry). These virtual MOs are thus responsible for the propagation of spin−orbit effects to the light atom via the FC mechanism, see MOs 158* and 161* in Figure 5.

According to eq 5, Ir d-AO contributions should be important for both the occupied and the virtual σ^{SO}-active MOs. As shown in Figure 4, changes of the virtual MO 156* should have a negligible effect on the $\Delta\sigma^{SO}$, since d-character of MO 156* (as well as nitrogen sp character and energy) is almost independent of the bond stretching (cf., Table S1 of the Supporting Information). In contrast, the iridium d-character of MO 139 is reduced by 19% and that of MO 140 increases by 20% (Figure 4). Modulations of contributions to σ^{SO} for the corresponding transitions from MO 139 and MO 140 parallel this trend: a decrease of −13 ppm for MO 139 and an increase of +9 ppm for MO 140 were calculated. It is clear that the sign of changes in σ^{SO} upon structural distortion is related exclusively to the changes of the d-character of *occupied* orbitals shown in Figure 4.

The σ^{SO}-active MOs 151 and 152 are nearly degenerate metal−ligand π-antibonding MOs with a significant Ir d_{xz} and d_{yz} character. This near-degeneracy also leads to similar contributions to $\Delta\sigma^{SO}$ from 151 → 158* and 152 → 158* magnetic couplings as well as from 151 → 161* and 152 → 161* magnetic couplings, where σ-antibonding MOs 158* and 161* have strong d_{z2} and d_{x2-y2} character, cf. Figure 5 and Table S2. However, while there is a substantial similarity within each pair of MO-MO* magnetic couplings, there is a large difference between the two pairs. Whereas magnetic couplings of MO 151 and 152 with MO 158* are connected with an increase in $\Delta\sigma^{SO}$, the couplings of the same occupied orbitals with MO 161* are responsible for a decrease in $\Delta\sigma^{SO}$. This reverse behavior cannot be rationalized by changes in the MO-MO* energy gap, see Figure 5 and Table S2 in the Supporting Information. Rather, it is consistent with an increase (MO 158*) and a decrease (MO 161*) in the d-character of the σ^{SO}-active virtual MO, cf. Figure 5. Thus, in this particular case, the sign of $\Delta\sigma^{SO}$ upon structural distortion is related to the changes of the d-character of *virtual* orbitals.

Note that Figures 4 and 5 show changes in the selected MO → MO* magnetic couplings demonstrating the most important trends. The sum of modulations given in Figures 4 and 5 is not equal to the total $\Delta\sigma^{SO}$. A full list of sizable contributions,

dx.doi.org/10.1021/ct400726y | J. Chem. Theory Comput. 2014, 10, 1489−1499

summing up to the total $\Delta\sigma^{SO}$, is given in Tables S1 and S2 of the Supporting Information.

To summarize, all three factors − the s-character of the LA in the HA-LA bonding, the energy gaps, and the d-character of the transition-metal HA of both occupied and virtual MOs (not necessary the HA-LA bonding MOs) − play important roles in the SO/FC mechanism of the HALA effect on the NMR chemical shifts. These factors are part of one physical mechanism, cf. eq 1, and interfere by strengthening or canceling each other, depending on the particular bonding situation. Whereas the role of s-character of the light atom as well as the energy gap have been investigated in detail, the importance of the metal d character is emphasized and analyzed here systematically for the first time.

3.4. Generalization for Molecules 1−8: Tuning Metal d-Character and σ^{SO} via *trans* Substituent. The analysis given in Section 3.3 demonstrated the important role of the iridium d-orbital character of the σ^{SO}-active MOs for the total SO-HALA shift of N9. Provided that the changes in energy gaps are either small or canceling each other, and ligand s-character in bonding remains constant, σ^{SO} should be directly proportional to the metal d-orbital participation in occupied and virtual σ^{SO}-active MOs. From the orbital-interaction point of view of bonding it follows that increasing the weight of the d orbitals in frontier MOs should be reflected also in the lower-lying, σ-bonding MOs. This should be observable both in canonical, delocalized orbital representation and in a localized, e.g., NBO representation of σ-bonding MOs. Thus, it appears that, abandoning the other influences, σ^{SO} should be directly proportional to the d-character of the Ir−N bonding NBO.

The latter hypothesis was tested via studying the σ^{SO} vs the d-character of the Ir−N bonding by using NBO (i) by stretching the Ir−S bond length in complex **1** (results not shown) and (ii) by changing the *trans* substituent using a testing set of iridium complexes (**2**−**8**) derived from IrBAP (**1**), Figure 2.

The testing set involves complexes with structurally different sulfur based ligands (**1**, **2**, **3**, **5**, **7**) complemented by their oxygen analogs (**4**, **6**, **8**). This allows us to compare two basic types of ligands, "soft" (sulfur based) and "hard" (oxygen based), introducing also different Ir−S (Ir−O) bond lengths (2.10−2.23 Å). As clear from Figure 6 and Table S3, the changes in iridium d-orbital contribution to the Ir−N bond are in a perfect correlation with observed changes in σ^{SO} of N9, even from a quantitative point of view (see the green squares and dashed line in Figure 6). We note that the s-character of N9 in the Ir−N bond remains basically intact along the series, see Figure 6. This suggests a more general validity of the proposed correlation between the d-character of bonding and σ^{SO}, which we below refer to as the Bonding D-Character (BDC) approach, even for the complexes with rather different *trans* ligands (e.g., water vs thiazen).

The correlation between the d-character of the HA-LA bond and σ^{SO} of the ligand atom allows for predicting the absolute values of σ^{SO} for complexes with different *trans* substituent and the same central atom. The predictive power of this approach is characterized by the RMSD value of ∼3.3 ppm, achieved for structurally heterogeneous *trans* substituents of complexes **1**−**8**, as is shown in the Supporting Information (Table S3). When the molecules with similar *trans* ligands, for example, **6** and **8**, are considered, the deviation between the BDC-predicted and SO-ZORA calculated σ^{SO} decreases down to 1.5 ppm. To explore further the general importance of the d-character of

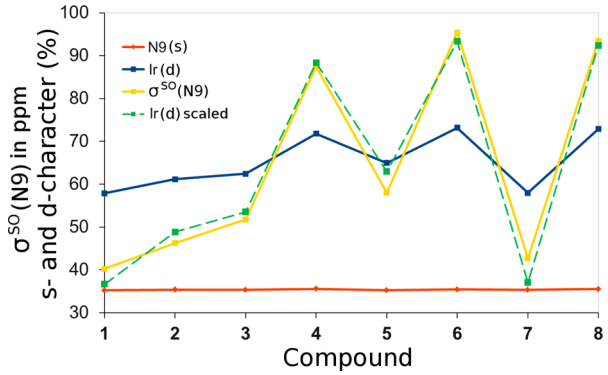

Figure 6. The σ^{SO}(N9) calculated at the PBE40/TZP/SO-ZORA level, the N9(s) and Ir(d) characters of the Ir−N bond (calculated at the PBE40/TZP/SR-ZORA level) in complexes **1**−**8**. The green squares (dashed line) represent the Ir d-character in the Ir−N bond uniformly scaled as y(green squares) = 3.71*Ir(d) − 178.1 to overlap with σ^{SO} values (see Table S3 of the Supporting Information). The points are connected by lines for better clarity.

bonding for σ^{SO}, additional calculations for square-planar platinum(II) complexes were performed, and the results are shown in Figure S5. These results indicate more general validity of our findings for different geometries (octahedral, square-planar) and the types of central atom (Ir, Pt). Thus, the proposed BDC approach allows for predicting the σ^{SO} for structure-related complexes with a good accuracy (using simple model compound and NBO analysis of bonding). This can be utilized in the future for estimating the σ^{SO} in large, computationally demanding systems (e.g., cisplatin drugs bonded to DNA).

3.5. EPR Parameters for Monovalent Cations 1−6. Let us now turn to the EPR parameters calculated for complexes **1**−**6** oxidized to monovalent cations. The isotropic nitrogen hyperfine coupling constant, $A_{iso}(^{15}N9)$, is determined by the spin populations of individual nitrogen atomic orbitals. There are two mechanisms how the spin population of nitrogen AOs can arise: the spin-delocalization contribution, i.e., spin population of nitrogen orbitals generated directly by the SOMO, and the spin-polarization contribution that produces spin population of nitrogen AOs via spin-polarized, nominally doubly occupied MOs.[49]

In our case, the interaction of the metal d_{yz} component of the SOMO with nitrogen $2p_y$ AO is symmetry-allowed, thus a nonzero spin population is induced in nitrogen p_y-based orbital. This spin-delocalization-induced population in nitrogen p_y-based orbital then spin-polarizes nitrogen s orbitals, which give a nonzero expectation value of the FC operator at the nitrogen nucleus, and contributes thus to the hyperfine coupling.[49] The amount of spin population, and hence the magnitude of the nitrogen hyperfine coupling constant, should be directly proportional to the metal d-character[60] and nitrogen p-character[64] of the metal−ligand π-antibonding SOMO, hence also to the d-character of the metal−ligand π-bonding MO. The d-character of metal−ligand π-bonding MO can be expected to parallel that of the metal−ligand σ-bonding MO. This is indeed the case, and the dependence of $A_{iso}(^{15}N9)$ on the metal d-character of the Ir−N bond is essentially perfect (see Figure 7).

The g-tensors of these systems are characterized by high rhombicity (Table S4 of the Supporting Information), which, however, originate in a predominant artificial localization of an unpaired electron in one of the two almost degenerate d_{xz}- and

dx.doi.org/10.1021/ct400726y | J. Chem. Theory Comput. 2014, 10, 1489−1499

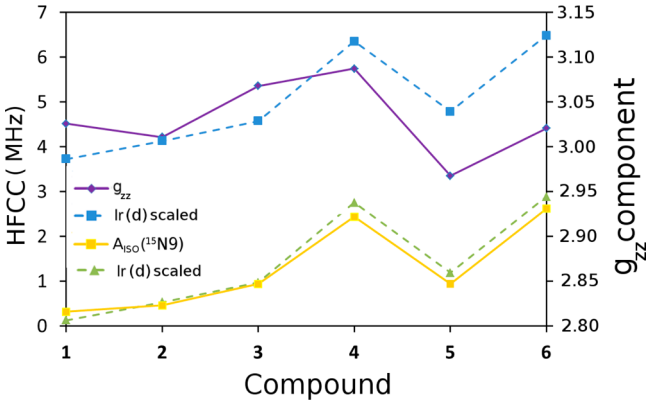

Figure 7. The $A_{iso}(^{15}N9)$ and g_{zz} for monovalent cations of complexes **1**−**6** (calculated at the PBE40/TZP/SO-ZORA level). The blue squares and green triangles (dashed lines) represent the Ir(d) of the Ir−N bond (calculated at the PBE40/TZP/SR-ZORA level) uniformly scaled and offsetted as y(green triangles) = 0.2*Ir(d) − 11.37 or y(blue squares) = 0.2*Ir(d) − 14.97 to overlap with $A_{iso}(^{15}N9)$ or g_{zz}, respectively. The points are connected by lines for better clarity. For g-tensor values, see Table S4 in the Supporting Information.

d_{yz}-based frontier orbitals in the SOMO region. The correct description of these systems would require a multiconfiguration treatment. However, the g_{zz} principal component (unlike the g_{xx} and g_{yy} components) should not be influenced dramatically by this artificial rhombicity.

Within our single-determinant description, the d^5 system possesses a single unpaired electron occupying d_{yz}-based MO 153. Considering the g_{zz} greater than 2.0023 (cf. Table S4),[65] the couplings of SOMO with the doubly occupied MOs contributing to the g_{zz} must dominate. Indeed, the magnetic couplings of SOMO with the d_{xz}- and d_{xy}-based iridium orbitals 152 and 151 provide a major contribution to the g_{zz} component. Thus, the d-character of MOs 151 and 152 influences the g_{zz} component of the EPR g-tensor in a similar way as the d-character of the analogous occupied orbitals influences the σ^{SO}-tensor in the related closed-shell systems (see Figure 5). Presuming that the change in the total metal d-orbital occupation correlates with the change in d-character of the HA-LA bond, the g-tensor should partially reflect the modulation of metal d-character of the bond. This is indeed the case, cf. Figure 7.

Thus, the qualitative electronic structure − spectroscopy relationships valid for the EPR g-tensor and A-tensor possess counterparts in the σ^{SO}-tensor. This turns out to be the case also for the dependence on the degree of covalence in a bond, often estimated in EPR spectroscopy from the g-tensor and hyperfine tensor components.[50,66] Because the bonding in TM complexes is realized mainly through d-orbitals of the metal and the bonding MOs are in general localized more on ligands, a higher covalence is connected with the higher metal d-character of bonding MOs, which in turn determines the size of σ^{SO}. Particularly, it has been demonstrated that the σ^{SO} of the LA correlates with the HA d-character of bonding (Figure 6) in the similar way as some EPR parameters do (Figure 7). Hence, the σ^{SO} in closed-shell compounds seems to be modulated by the electronic factors resembling those influencing the EPR parameters in related open-shell systems (cf. Section 3.2). We demonstrated that σ^{SO} is proportional to the d-character of the metal−ligand bond. Similar correlation between σ^{SO} and the f-character of bonding, suggested very recently for the uranium complexes,[67] indicates that the relationships discussed in this paper can be further generalized for compounds outside the regular transition-metal complexes.

The analogy between the EPR parameters and the σ^{SO}-tensor might be in the future employed to develop, in the context of NMR, further relationships between the structure, the bonding, and σ^{SO} as counterparts of corresponding relationships for the EPR g-tensor and A-tensor. Indeed, the individual components of electronic g-tensor are known to be correlated not only to the separation of the occupied and virtual MOs but also to the relative strength of multiple π vs σ bonds or (by means of comparing the g- and A-tensor orientations) to the tendency of complexes to bending.[50,65]

4. CONCLUSIONS

The orbital mechanism of the spin−orbit induced contribution to the nuclear shielding constants (σ^{SO}) of light ligand atoms in the transition-metal complexes was systematically investigated using a set of model d^6 iridium complexes. Although significant differences in σ^{SO} of the light atom were observed upon stretching or chemically modifying the metal−ligand bond located *trans* to the NMR spectator light nucleus, we demonstrate that the Fermi-contact term, dependent on the s-contribution of the light atom in the metal−ligand bond, is nearly intact. This is in a striking contrast to the situation in main-group compounds, where the change in σ^{SO} usually corresponds to the variation of the latter parameter. Similarly, the energy gaps between occupied and virtual molecular orbitals were shown not to be the only parameter responsible for the sign of modulation of σ^{SO}. We demonstrate and explain here for the first time the crucial importance of the transition-metal d-orbital contribution to both occupied and virtual MOs involved in the SO/FC mechanism of σ^{SO}.

Further, we show that the conclusions formulated from canonical molecular orbital analysis of σ^{SO} can be extended to the importance of the transition-metal d-orbital admixture in the localized HA-LA bonding MOs. The proposed Bonding D-Character (BDC) approach allows us to predict σ^{SO} in a class of structurally related complexes to a very good accuracy. Our analysis also provides a useful link of σ^{SO}-tensor to the g- and A-tensors of the EPR spectroscopy, whose mechanisms are shown to be analogous to the SO/FC nuclear shielding mechanism in the NMR spectroscopy. For the known relationship between the degree of covalence in a bond and the g-tensor, we found an analogy in terms of σ^{SO} that is, in our systems, also found proportional to the degree of covalence of the HA-LA bond. We assume that other known qualitative relationships valid for EPR g- and A-tensors and structure/bonding can be extended also to the SO-HALA effects in NMR spectroscopy.

■ ASSOCIATED CONTENT

Supporting Information

Figure S1: Qualitative description of bonding in IrBAP, Figure S2: visualization of the spin density induced by perturbation at N9, Figure S3: visualization of the σ-bonding MOs corresponding to Ir−N bond, Figure S4: energies of occupied and virtual σ^{SO}-active MOs, Figure S5: metal d-character of the HA-LA bonding and the σ^{SO} of the ligand atom for a series of square-planar Pt(II) complexes, Tables 1−3: MO → MO* magnetic couplings analysis including ligand and metal characters of σ^{SO}-active MOs, Table 4: EPR g-tensor

parameters. This material is available free of charge via the Internet at http://pubs.acs.org.

AUTHOR INFORMATION

Corresponding Authors

*E-mail: marketa@chemi.muni.cz (M.L.M.).
*E-mail: rmarek@chemi.muni.cz (R.M.).

Notes

The authors declare no competing financial interest.

ACKNOWLEDGMENTS

This work was supported by the Czech Science Foundation (P206/12/0539) and carried out at CEITEC − Central European Institute of Technology with research infrastructure supported by the project CZ.1.05/1.1.00/02.0068 financed from the European Regional Development Fund. The access to computing and storage facilities owned by parties and projects contributing to the National Grid Infrastructure MetaCentrum, provided under the program "Projects of Large Infrastructure for Research, Development, and Innovations" (LM2010005), and the CERIT-SC computing and storage facilities, provided under the program Center CERIT Scientific Cloud, part of the Operational Program Research and Development for Innovations (CZ.1.05/3.2.00/08.0144), is acknowledged.

REFERENCES

(1) Autschbach, J. In *High Resolution NMR Spectroscopy*; Elsevier: Amsterdam, 2013; Vol. 3, pp 69−117.
(2) Nakagawa, N.; Sinada, S.; Obinata, S. *The 6th NMR Symposium*, Kyoto, 1967; p 8.
(3) Nomura, Y.; Takeuchi, Y.; Nakagawa, N. *Tetrahedron Lett.* **1969**, *10*, 639−642.
(4) Cheremisin, A. A.; Schastnev, P. V. *J. Magn. Reson.* **1969**, *40*, 459−468.
(5) Pyykkö, P.; Görling, A.; Rösch, N. *Mol. Phys.* **1987**, *61*, 195−205.
(6) Kaupp, M.; Malkina, O. L.; Malkin, V. G. *Chem. Phys. Lett.* **1997**, *265*, 55−59.
(7) Kaupp, M.; Malkina, O. L.; Malkin, V. G.; Pyykkö, P. *Chem.—Eur. J.* **1998**, *4*, 118−126.
(8) Kaupp, M. In *Relativistic Electronic Structure Theory II: Applications II, Theoretical and Computational Chemistry*; Schwerdtfeger, P., Ed.; Elsevier: Amsterdam, 2004; Chapter 9, pp 552−597, and references therein.
(9) Wolff, S.; Ziegler, T. *J. Chem. Phys.* **1998**, *109*, 895−905.
(10) Minaev, B.; Vaara, J.; Ruud, K.; Vahtras, O.; Ågren, H. *Chem. Phys. Lett.* **1998**, *295*, 455−461.
(11) Hegetschweiler, K.; Kuppert, D.; Huppert, J.; Straka, M.; Kaupp, M. *J. Am. Chem. Soc.* **2004**, *126*, 6728−6738.
(12) Hyvärinen, M.; Vaara, J.; Goldammer, A.; Kutzky, B.; Hegetschweiler, K.; Kaupp, M.; Straka, M. *J. Am. Chem. Soc.* **2009**, *131*, 11909−11918.
(13) Straka, M.; Kaupp, M. *Chem. Phys.* **2005**, *311*, 45−56.
(14) Yoshizawa, T.; Sakaki, S. *J. Comput. Chem.* **2013**, *34*, 1013−1023.
(15) Neto, A. C.; Ducati, L. C.; Rittner, R.; Tormena, C. F.; Contreras, R. H.; Frenking, G. *J. Chem. Theory Comput.* **2009**, *5*, 2222−2228.
(16) Truflandier, L. A.; Brendler, E.; Wagler, J.; Autschbach, J. *Angew. Chem., Int. Ed.* **2011**, *50*, 255−259.
(17) Pawlak, T.; Munzarová, M. L.; Pazderski, L.; Marek, R. *J. Chem. Theory Comput.* **2011**, *7*, 3909−3923.
(18) Burdett, J. K.; Albright, T. A. *Inorg. Chem.* **1979**, *18*, 2112−2120.
(19) Vícha, J.; Patzschke, M.; Marek, R. *Phys. Chem. Chem. Phys.* **2013**, *15*, 7740−7754.
(20) Shriver, D. F.; Atkins, P. W.; Langford, C. H. *Inorganic Chemistry*, 2nd ed.; Oxford University Press: Oxford, 1996; p 626.
(21) Kaupp, M.; Malkina, O. L.; Malkin, V. G. *J. Comput. Chem.* **1999**, *20*, 1304−1313.
(22) Un, S. *Inorg. Chem.* **2013**, *52*, 3803−3813.
(23) Vícha, J.; Maloň, M.; Veselá, P.; Humpa, O.; Strnad, M.; Marek, R. *Magn. Reson. Chem.* **2010**, *48*, 318−322.
(24) Vícha, J.; Demo, G.; Marek, R. *Inorg. Chem.* **2012**, *51*, 1371−1379.
(25) Perdew, J. P.; Burke, K.; Ernzerhof, M. *Phys. Rev. Lett.* **1996**, *77*, 3865−3868.
(26) Adamo, C.; Barone, V. *J. Chem. Phys.* **1999**, *110*, 6158−6169.
(27) Weigend, F.; Ahlrichs, R. *Phys. Chem. Chem. Phys.* **2005**, *7*, 3297−3305.
(28) Andrae, D.; Haeussermann, U.; Dolg, M.; Stoll, H.; Preuss, H. *Theor. Chim. Acta* **1990**, *77*, 123−141.
(29) TURBOMOLE V6.3 2011, a development of University of Karlsruhe and Forschungszentrum Karlsruhe GmbH, 1989−2007, TURBOMOLE GmbH, since 2007. Available from http://www.turbomole.com (accessed Feb 15, 2014).
(30) Klamt, A.; Schüürmann, G. *J. Chem. Soc., Perkin Trans. 2* **1993**, 799−803.
(31) van Lenthe, E.; Snijders, J. G.; Baerends, E. J. *J. Chem. Phys.* **1996**, *105*, 6505−6516.
(32) van Lenthe, E.; Ehlers, A. E.; Baerends, E. J. *J. Chem. Phys.* **1999**, *110*, 8943−8953.
(33) ADF2012, SCM, Theoretical Chemistry, Vrije Universiteit, Amsterdam, The Netherlands, http://www.scm.com (accessed Feb 15, 2014).
(34) Pye, C. C.; Ziegler, T. *Theor. Chem. Acc.* **1999**, *101*, 396−408.
(35) Hrobárik, P.; Hrobáriková, V.; Meier, F.; Repiský, M.; Komorovský, S.; Kaupp, M. *J. Phys. Chem. A* **2011**, *115*, 5654−5659.
(36) Malkin, V. G.; Malkina, O. L.; Reviakine, R.; Arbuznikov, A. V.; Kaupp, M.; Schimmelpfennig, B.; Malkin, I.; Repisky, M.; Komorovsky, S.; Hrobarik, P.; Malkin, E.; Helgaker, T.; Ruud, K. MAG-ReSpect, version 2.1; Universität Würzburg; Würzburg, Germany, 2010.
(37) Frisch, M. J.; Trucks, G. W.; Schlegel, H. B.; Scuseria, G. E.; Robb, M. A.; Cheeseman, J. R.; Scalmani, G.; Barone, V.; Mennucci, B.; Petersson, G. A.; Nakatsuji, H.; Caricato, M.; Li, X.; Hratchian, H. P.; Izmaylov, A. F.; Bloino, J.; Zheng, G.; Sonnenberg, J. L.; Hada, M.; Ehara, M.; Toyota, K.; Fukuda, R.; Hasegawa, J.; Ishida, M.; Nakajima, T.; Honda, Y.; Kitao, O.; Nakai, H.; Vreven, T.; Montgomery, J. A., Jr.; Peralta, J. E.; Ogliaro, F.; Bearpark, M.; Heyd, J. J.; Brothers, E.; Kudin, K. N.; Staroverov, V. N.; Kobayashi, R.; Normand, J.; Raghavachari, K.; Rendell, A.; Burant, J. C.; Iyengar, S. S.; Tomasi, J.; Cossi, M.; Rega, N.; Millam, J. M.; Klene, M.; Knox, J. E.; Cross, J. B.; Bakken, V.; Adamo, C.; Jaramillo, J.; Gomperts, R.; Stratmann, R. E.; Yazyev, O.; Austin, A. J.; Cammi, R.; Pomelli, C.; Ochterski, J. W.; Martin, R. L.; Morokuma, K.; Zakrzewski, V. G.; Voth, G. A.; Salvador, P.; Dannenberg, J. J.; Dapprich, S.; Daniels, A. D.; Farkas, Ö.; Foresman, J. B.; Ortiz, J. V.; Cioslowski, J.; Fox, D. J. Gaussian 09, Revision A.1; Gaussian, Inc.: Wallingford, CT, 2009.
(38) Faegri, K., Jr. *Theor. Chem. Acc.* **2001**, *105*, 252−258.
(39) NBO 5.0. Glendening, E. D.; Badenhoop, J. K.; Reed, A. E.; Carpenter, J. E.; Bohmann, J. A.; Morales, C. M.; Weinhold, F. Theoretical Chemistry Institute, University of Wisconsin, Madison, WI, 2001.
(40) Autschbach, J.; Zheng, S.; Schurko, R. W. *Conc. Magn. Reson.* **2010**, *36A*, 84−126.
(41) Chan, K. W.; Sau, Y. K.; Zhang, Q. F.; Wong, W. Y.; Williams, I. D.; Leung, W. H. *Eur. J. Inorg. Chem.* **2008**, 4353−4359.
(42) Gamero-Melo, P.; Melo-Trejo, P. A.; Cervantes-Vasquez, M.; Mendizabal-Navarro, N. P.; Paz-Michel, B.; Villar-Masetto, T. I.; Gonzalez-Fuentes, M. A.; Paz-Sandoval, M. A. *Organometallics* **2012**, *31*, 170−190.
(43) Vaara, J.; Manninen, P.; Lantto, P. In *Calculation of NMR and EPR Parameters*; Wiley-VCH: Weinheim, 2004; pp 209−226.
(44) Standara, S.; Maliňáková, K.; Marek, R.; Marek, J.; Hocek, M.; Vaara, J.; Straka, M. *Phys. Chem. Chem. Phys.* **2010**, *12*, 5126−5139.

(45) Malkin, V. G.; Malkina, O. L.; Salahub, D. R. *Chem. Phys. Lett.* **1996**, *261*, 335−345 The energy correction $\Delta E_{k\rightarrow a}^{0,xc}$ used in the SOS-DFPT approach of Malkin et al. has been omitted in the denominator of eq 1.
(46) Malkina, O. L.; Vaara, J.; Schimmelpfennig, B.; Munzarová, M.; Malkin, V. G.; Kaupp, M. *J. Am. Chem. Soc.* **2000**, *122*, 9206−9218.
(47) Belanzoni, P.; Baerends, E. J.; van Asselt, S.; Langewen, P. B. *J. Phys. Chem.* **1995**, *99*, 13094−13102.
(48) Belanzoni, P.; Baerends, E. J.; Gribnau, M. *J. Phys. Chem. A* **1999**, *103*, 3732−3744.
(49) Cano, J.; Ruiz, E.; Alvarez, S.; Verdaguer, M. *Comments Inorg. Chem.* **1998**, *20*, 27−56.
(50) Weil, A.; Bolton, J. R.; Wertz, J. E. *Electron Paramagnetic Resonance. Elementary Theory and Practical Applications*; John Wiley & Sons, Inc.: New York, 1994; pp 100−105.
(51) Patschkovskii, S.; Schreckenbach, G. In *Calculation of NMR and EPR Parameters*; Wiley-VCH: Weinheim, 2004; pp 513−515.
(52) Mabbs, F. E.; Collison, D. *Electron Paramagnetic Resonance of d Transition Metal Compounds*; Elsevier: Amsterdam, 1992; pp 338−441.
(53) Maki, A. H.; McGarvey, B. R. *J. Chem. Phys.* **1958**, *29*, 31.
(54) McGarvey, B. R. *Transition Met. Chem.* **1966**, *3*, 89.
(55) Case, D. A.; Karplus, M. *J. Am. Chem. Soc.* **1977**, *99*, 6182−6194.
(56) Mattar, S. M.; Sammynaiken, R. *J. Chem. Phys.* **1997**, *106*, 1094−1111.
(57) Knight, L. B.; Babb, R.; Ray, M.; Banisaukas, T. J., III; Russon, L.; Dailey, R. S.; Davidson, E. R. *J. Chem. Phys.* **1996**, *23*, 105.
(58) Smith, D. W. *J. Chem. Soc. A* **1970**, 3108.
(59) Munzarová, M. L. *Electron Paramagnetic Resonance*. In *Comprehensive Inorganic Chemistry*, 2nd ed.; Elsevier: Amsterdam, 2013; pp 359−380.
(60) Munzarová, M.; Kubáček, P.; Kaupp, M. *J. Am. Chem. Soc.* **2000**, *122*, 11900−11913.
(61) Ramsey, N. F. *Phys. Rev.* **1950**, *78*, 699−703.
(62) Wiberg, K. B.; Hammer, J. D.; Zilm, K. W.; Cheeseman, J. R.; Keith, T. A. *J. Phys. Chem. A* **1998**, *102*, 8766−8773.
(63) Autschbach, J.; Zheng, S. *Magn. Reson. Chem.* **2008**, *46*, S45−S55.
(64) McConnell, H. M. *J. Chem. Phys.* **1956**, *24*, 764−766.
(65) Symons, M. C. R. *Chemical and Biochemical Aspects of Electron-Spin Resonance Spectroscopy*; Van Nostrand Reinhold: Wokingham, 1978; pp 136−139.
(66) Raynor, J. B.; Jelizakowa, B. G. *J. Chem. Soc., Dalton Trans.* **1982**, 1185−1189.
(67) Seaman, L. A.; Hrobárik, P.; Schettini, M. F.; Fortier, S.; Kaupp, M.; Hayton, T. W. *Angew. Chem., Int. Ed.* **2013**, *52*, 3259−3263.